Photodissociation of acryloyl chloride in the gas phase

YANG ChunFan, WU WeiQiang, LIU KunHui, WANG Huan & SU HongMei[*]

State Key Laboratory of Molecular Reaction Dynamics; Beijing National Laboratory for Molecular Sciences (BNLMS); Institute of Chemistry, Chinese Academy of Sciences, Beijing 100190, China

The 193 nm photodissociation dynamics of $CH_2CHCOCl$ in the gas phase has been examined with the technique of time-resolved Fourier transform infrared emission (TR-FTIR) spectroscopy. Vibrationally excited photofragments of CO ($v \leqslant 5$), HCl ($v \leqslant 6$), and C_2H_2 were observed and two photodissociation channels, the C–Cl fission channel and the HCl elimination channel have been identified. The vibrational and rotational state distributions of the photofragments CO and HCl have been acquired by analyzing their fully rotationally resolved $v \rightarrow v-1$ rovibrational progressions in the emission spectra, from which it has been firmly established that the mechanism involves production of HCl via the four-center molecular elimination of $CH_2CHCOCl$ after its internal conversion from the S_1 state to the S_0 state. In addition to the dominant C–Cl bond fission along the excited S_1 state, the $S_1 \rightarrow S_0$ internal conversion has also been found to play an important role in the gas phase photolysis of $CH_2CHCOCl$ as manifested by the considerable yield of HCl.

TR-FTIR, photodissociation, vibrational and rotational state distribution, four-center elimination, internal conversion
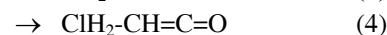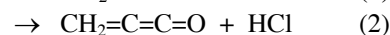
1   Introduction

The photochemistry of α,β unsaturated carbonyl compounds is of particular interest to a variety of researchers in the field of organic [1], biomedical [2], and physical chemistry because these compounds serve as building blocks for further functionalization via various photochemical reactions. Besides the well known photoinduced cycloaddition reactions [3–6] characterized by the ring closure of the C=C–C=O moiety, photoexcitation can also result in α bond cleavage and (1,n) sigmatropic rearrangements [7–10]. However, these photodissociation and photoisomerization reactions have been less widely studied, despite their importance in understanding the photochemistry of α,β unsaturated carbonyl compounds. In this work, we study the photodissociation reactions of the simplest α,β unsaturated acyl chloride, acryloyl chloride ($CH_2CHCOCl$).

$CH_2CHCOCl$ is known to exist in two conformers, a more stable planar *S-trans* form and a less stable *S-cis* form, as shown in Scheme 1. Several experimental investigations of its structure have been reported [11–14]. The energy difference between the *S-trans* and *S-cis* forms and the barrier to isomerization have been determined to be less than 1.0 and 3.5 kcal mol^{-1}, respectively [11–14].

Butler *et al*. have recorded the emission spectra of acryloyl chloride and elucidated the dominant electronic character of the excited state reached by the optical transition at 199 nm. By examining the C=C and C=O overtones as well as various combination bands in the emission spectra, and aided by configuration interaction with single excitation (CIS) calculations, the excited state reached by 199 nm excitation was identified to possess a mixed C=C/C=O π character. The electronic excitation may lead to four possible photodissociation or photoisomerization channels as follows:

$$CH_2CHCOCl + h\nu \rightarrow CH_2CHCO + Cl \qquad (1)$$
$$\rightarrow CH_2=C=C=O + HCl \qquad (2)$$
$$\rightarrow CH_2=CH + ClCO \qquad (3)$$
$$\rightarrow ClH_2\text{-}CH=C=O \qquad (4)$$

*Corresponding author (email: hongmei@iccas.ac.cn)

In the gas phase when excited with a 193 nm laser, $CH_2CHCOCl$ was found by Butler and collaborators to undergo primarily C–Cl bond fission (channel (1)) [7–9]. Using photofragment translational spectroscopy, two cases were observed: one produced Cl atoms with high kinetic recoil energy and was inferred to involve a predissociation via a repulsive state in the C–Cl bond; the other produced low energy Cl atoms and was suggested to proceed in the ground state after internal conversion from the excited electronic state. In both cases, the co-fragment CH_2CHCO radical was found to possess sufficient internal energy (23 to 68 kcal mol^{-1}) to overcome the barrier to further dissociation to give CH_2CH and CO. This barrier was calculated by the method of G3//B3LYP to be 22.4 kcal mol^{-1} and latter was determined to be 21±2 and 23 ±2 kcal mol^{-1} respectively for the two resonant structures $CH_2CHCO\cdot$ and $\cdot CH_2CHCO$ by means of two-dimensional product velocity map imaging experiments [9].

Besides the major C–Cl bond fission channel (1), Butler *et al.* also observed some formation of HCl and proposed that the HCl elimination channel (2) can occur in the ground state following internal conversion. The kinetic energy of HCl was measured to have a maximum at 5 kcal mol^{-1} and extend to 49 kcal mol^{-1}, from which the metastable co-product $CH_2=C=C=O$ was estimated to have sufficient internal energy to overcome the barrier of 39.5 kcal mol^{-1} and undergo secondary dissociation. They also found considerable vibrational excitation of the HCl, and estimated its internal energy to be roughly 23 kcal mol^{-1}.

In the Ar matrix at $\lambda \geq 310$ nm, the *cis* to *trans* isomerization, and the photoisomerization of 1,3-Cl migration producing 3-chloro-1,2-propenone (ClCH$_2$–CH=C=O), i.e.,

channel (4), were the only two observed pathways [10]. At $\lambda \geq 230$ nm, the 1,3-Cl migration was accelerated and the primary product ClCH$_2$–CH=C=O dissociated further via two pathways: one involved the release of CO and 2-chloroethylidene (ClCH$_2$C:) which promptly isomerized to vinyl chloride (CH$_2$CHCl); the other involved elimination of HCl to produce the unstable 1,2-propadienone (CH$_2$= C=C=O) which subsequently dissociated into CO and C_2H_2. CO, HCl, CH$_2$CHCl, and C_2H_2 were observed as final stable products in the FTIR spectrum following the irradiation at $\lambda \geq 230$ nm of CH$_2$CHCOCl in the Ar matrix. These processes are summarized in Scheme 1.

In response to these experiments, a few complementary *ab initio* calculations have been performed. Early studies only focused on the structures of CH$_2$CHCOCl in the ground state with the exception of the CIS calculations of the properties of the excited states referred to above [7]. Recently, the potential energy surfaces of isomerization and dissociation reactions of CH$_2$CHCOCl in the S_0, T_1, T_2 and S_1 states have been mapped using DFT, CASSCF, MP2 and MR-CI calculations by Fang *et al.* [15]. It was found that there exists an $S_1/T_1/T_2$ three-surface intersection which results in fast intersystem crossing (ISC). Thus, nonadiabatic processes were suggested to be extensively involved in the photochemistry of CH$_2$CHCOCl. For example, the photoinduced 1,3-Cl migration reaction was suggested to follow a route involving the T_1 state after an efficient intersystem crossing of $S_1 \rightarrow T_1$ because of the significantly lower barrier of 18.4 kcal mol^{-1} compared with that in the S_0 state, 41.8 kcal mol^{-1}. On the basis of the calculations, the photochemical reaction mechanisms for irradiation at
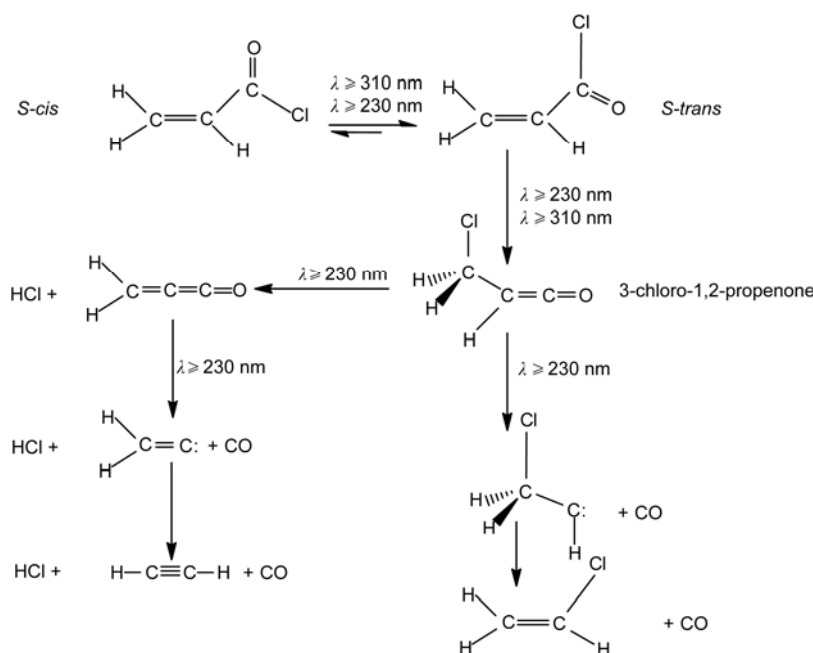
Scheme 1

230–310 nm were proposed which can provide reasonable explanations for the experimental findings. When excited at 310 nm, the photon energy is not sufficient to overcome the barrier to C–Cl bond fission in the S_1 state and thus $S_1 \rightarrow T_1$ intersystem crossing was suggested to be the dominant process followed by 1,3-Cl migration to afford 3-chloro-1,2-propenone (ClCH$_2$–CH=C=O) in the T_1 state. On irradiation of gaseous CH$_2$CHCOCl with higher photon energy of 230 nm, C–Cl bond fission was suggested to be the exclusive primary channel.

As indicated in these previous investigations, nonadiabatic processes, internal conversion and intersystem crossing play significant roles affecting the photodissociation or photoisomerization of CH$_2$CHCOCl. The photolysis channels tend to occur in the lower electronic states via internal conversion or intersystem crossing processes, though initially involving excitation to a higher state. But there appear to be some disagreements regarding the reaction mechanisms postulated on the basis of previous studies. For example, the HCl elimination channel (2) was suggested to proceed in the highly vibrationally excited ground S_0 state following internal conversion of CH$_2$CHCOCl by Butler and coworkers [8] but Ar-matrix experiments [10] were indicative of a mechanism involving HCl formation from the 3-chloro-1,2-propenone (ClCH$_2$–CH=C=O) which is produced from the 1,3-Cl migration of CH$_2$CHCOCl.

To examine the photodissociation dynamics of CH$_2$CHCOCl which is complicated by the nonadiabatic processes, we focus on probing the internal energy distribution of photofragments from which the key mechanistic information can be derived. The fragments from 193 nm photodissociation of CH$_2$CHCOCl in the gas phase were detected by means of step-scan time-resolved Fourier transform infrared (TR-FTIR) emission spectroscopy. Because of its broad band advantage and nanosecond time resolution, TR-FTIR spectroscopy is an effective technique probing multiple IR-active reaction products in real time and thus is especially suitable for studying multichannel photochemical reactions such as that of CH$_2$CHCOCl. The vibrationally excited photofragments CO ($v \leqslant 5$), HCl ($v \leqslant 6$), and C$_2$H$_2$ were observed and two photodissociation channels, the C–Cl fission channel (1) and the HCl elimination channel (2), have been identified. The vibrational and rotational state distributions of the photofragments CO and HCl were acquired by analyzing the fully resolved $v \rightarrow v-1$ progressions of rovibrational transitions in the emission spectra, from which a mechanism has been firmly established involving the production of HCl via the four-center molecular elimination of CH$_2$CHCOCl after its internal conversion from the S_1 state to the S_0 state. In addition to the dominant C–Cl bond fission along the excited S_1 state, the $S_1 \rightarrow S_0$ internal conversion is also found to play important roles in the gas phase photolysis of CH$_2$CHCOCl as manifested by the considerable yield of HCl.

2 Experimental

The reaction products were monitored by step-scan, time-resolved Fourier transform IR emission spectroscopy [16, 17]. The instrument comprises a Nicolet Nexus 870 step-scan FTIR spectrometer, Lambda Physik (Compex-Pro102F) excimer laser and a pulse generator (Stanford Research DG535) to initiate the laser pulse and achieve synchronization of the laser with data collection, two digitizers (an internal 100 kHz 16-bit digitizer and an external 100 MHz 14-bit GAGE 8012A digitizer) which offer fast time resolution and a wide dynamic range as needed, and a personal computer to control the whole experiment. High resolution IR emission spectra with a good ratio of signal to noise were obtained by averaging four sets (0.5 cm^{-1}) or fourteen sets (4 cm^{-1}) of spectra in separate experiments under similar conditions. The detector used was a liquid nitrogen cooled InSb detector.

The reaction was initiated in a stainless steel flow reaction chamber. The photolysis beam from an ArF excimer laser at 193 nm with a fluence of 40–45 mJ cm^{-2} was directed into the reaction chamber and further reflected by a pair of parallel multi-layer coated mirrors (reflectivity $R > 0.80$ at 193 nm) inside it in order to increase the photolysis zone. The samples entered the flow chamber 1 cm above the photolysis beam via needle valves. The chamber was pumped by an 8 L s^{-1} mechanical pump and the stagnation pressure of the chamber was measured by a MKS capacitance monometer. The constant pressure of sample was maintained by adjusting the pumping speed and the needle valves. The flow rate was fast enough to replenish the sample at each laser pulse running normally at a repetition rate of 10 Hz as described in detail previously [16, 17]. Transient emitted infrared fluorescence was collected by a pair of gold-coated Welsh-Cell spherical mirrors and collimated by a CaF$_2$ lens to the step-scan Fourier spectrometer (Nicolet Nexus 870).

CH$_2$CHCOCl (Alfa, > 96%) was used without further purification. In the gaseous experiments, the pressure of CH$_2$CHCOCl in the chamber was kept about 0.05 torr. The buffer gas Ar (Oriental Center Gas, 99.999%) was added in the entrance port for the photolysis beam to suppress the formation of a solid carbon deposit on the fused quartz window. With Ar purging, the total pressure of system was maintained at about 0.11 torr.

3 Results and discussion

3.1 Experimental detection of photofragments

Figure 1 shows representative IR emission spectra of the photofragments from the photolysis at 193 nm of a flowing mixture of CH$_2$CHCOCl (0.05 torr) and the buffer gas (0.06 torr Ar). Intense emission bands originating from the vibra-
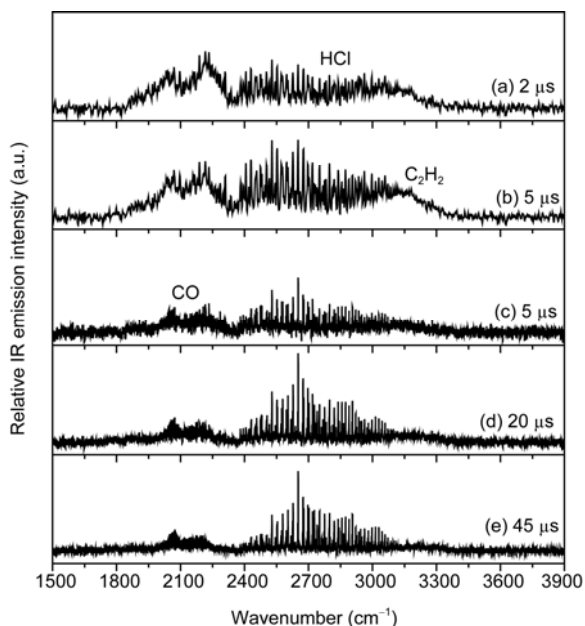
Figure 1 Product TR-FTIR emission spectra from the photolysis of CH$_2$CHCOCl taken at typical delay times from 2 to 45 μs after initiation of the reaction by a 193 nm laser. All the spectra were collected using a high sensitivity liquid nitrogen InSb detector. (a) and (b) Spectral resolution of 4 cm^{-1}; (c)–(e) spectral resolution of 0.5 cm^{-1}

tionally excited photofragments were observed immediately after laser photolysis at 2 μs and these molecules were subsequently quenched to lower vibrational states.

IR emission spectra record the infrared fluorescence emitted from vibrationally excited species due to several sets of vibrational transitions $v{\rightarrow}v{-}1$ and thus the bands are generally much broader than normal static IR absorption spectra and the peak center exhibits a slight red shift relative to the fundamental frequency position ($1{\rightarrow}0$). As shown in the 4 cm^{-1} resolution spectra in Figure 1 (a) and (b), there are three broad IR emission bands spanning 1800–2300, 2400–3200, and 2900–3400 cm^{-1}. To assign these bands more precisely, higher resolution (0.5 cm^{-1}) spectra were collected and are shown in Figure 1 (c) to (e). Clearly, two bands are well rotationally resolved with 0.5 cm^{-1} resolution and thus can be unambiguously assigned based on their rotational structure: the 1800–2300 cm^{-1} band and the 2400–3200 cm^{-1} band are ascribed to rovibrational transitions of CO ($v{\rightarrow}v{-}1$) and HCl ($v{\rightarrow}v{-}1$), respectively. The third band from 2900–3400 cm^{-1} is still irresolvable at a resolution of 0.5 cm^{-1} indicating that it arises from polyatomic molecules. According to its spectral position, this band can be attributed to C$_2$H$_2$ v_3 (fundamental frequency at 3289 cm^{-1}).

Laser power dependence of the photofragment yields was measured in the power range of 24–64 mJ.cm^{-2}. For HCl and C$_2$H$_2$, the laser power dependence was 1.1 ± 0.1 indicating that these fragments arise from one-photon photolysis processes. For CO, the measured laser power depend-

ence was 1.2 ± 0.2 indicating that this fragment also arises mainly from a one-photon process.

3.2 Rovibrational state distribution of CO and HCl

TR-FTIR emission spectra can provide an almost complete vibrational and rotational state distribution because they record the broad band spectra due to several $v{\rightarrow}v{-}1$ progressions of rovibrational transitions. The state distribution can be acquired by spectral fitting to experimental IR emission spectra using nonlinear least-squares fitting procedures [16]. For the three observed photofragments, the diatomic molecules CO and HCl show rotationally resolved spectra from which unique fitting results and thus meaningful state distribution can be obtained, whereas the spectra of the polyatomic C$_2$H$_2$ are simply featureless and only show an unresolved contour resulting from superimposition of numerous rovibrational transitions. Therefore, only the rotationally resolved IR emission spectra of the diatomic products CO and HCl were analyzed by spectral fitting.

Spectral fitting was performed for CO and HCl using the spectral constants of these two molecules and a nonlinear least-squares fitting program which has been described in detail elsewhere [16]. Representative fitting results for two particular time slices are displayed in Figure 2, demonstrating further that these two bands can be ascribed to CO and HCl molecules. The spectral fitting yields the vibrational populations and rotational temperature.

As shown in Table 1, the photofragments HCl and CO only possess moderate rotational excitation. At 2 μs for the photolysis of 0.05 torr CH$_2$CHCOCl in the buffer (0.06 torr Ar), nearly collisionless conditions are acquired and thus the rotational excitation is not yet quenched. Temperatures of 1500 ± 150 and 4000 ± 500 K should be very close to the nascent rotational temperatures of HCl and CO, respectively. The corresponding average rotational energies are 3.0 and 7.9 kcal mol^{-1} for HCl and CO, respectively. At later times, the molecules undergo fast rotational relaxation and after 45 μs, the rotational excitation has been completely thermalized.

As an example to show the reliability of the above spectral fitting, the rotationally resolved IR emission bands of

Table 1 Rotational temperature of the photofragments HCl and CO obtained from spectral fitting

Time (μs)	Rotational temperature (K)	
	HCl	CO
2	1500±150	4000±500
5	900±100	3000±500
10	450±50	2000±400
15	450±50	1000±400
25	450±50	800±200
35	450±50	500±100
45	350±50	350±50

HCl were analyzed by assigning each rovibrational transition manually as shown in Figure 3. Partial assignments for HCl are shown as stick diagrams, based on spectral parameters reported by Aruman *et al.* [18] and Coxon-Roychowdhury [19] values of J'' (the value of J in the lower vibrational energy level) corresponding to each $v \rightarrow v-1$ progression are indicated. The spectrum clearly illustrates that HCl is only moderately rotationally excited ($J_{max} = 19$) with obvious P bandheads for $v = 1-5$. This agrees with the low rotational temperature (1500 ± 150 K) for HCl derived from the spectral fitting. In contrast, highly rotationally excited HCl formed in the photodissociation of vinyl chloride at 193 nm is characterized by high J values ($J_{max} = 42$) [20].

The spectral fitting can also yield the populations in each vibrational level. For example, the spectral fittings displayed in Figure 2 afforded populations of 1.0/0.88/0.28/0.16/0.17/0.33 for the vibrational levels $v' = 1-6$ of HCl and 1.0/0.59/0.31/0.20/0.13 for the vibrational levels $v' = 1-5$ of CO at 5 µs. These populations can be described by a Boltzmann vibrational distribution as shown in Figure 4. The population of the ground state ($v = 0$) is obtained by extrapolating the Boltzmann plot to $v = 0$. The equation $<E_v> = \sum N_v E_v / \sum N_v$ is used to obtain average vibrational energy, where N_v is the vibrational population of CO(v) or HCl(v) and E_v (including zero vibrational energy) is the vibrational energy at vibrational level v. As shown in Table 2, the average vibrational energies measured at 2 µs, 20.8 and 10.7 kcal mol^{-1} for HCl and CO respectively, are presumably

Table 2 Vibrational temperature and average vibrational energy of products CO and HCl from the photodissociation of CH$_2$CHCOCl at typical delay times

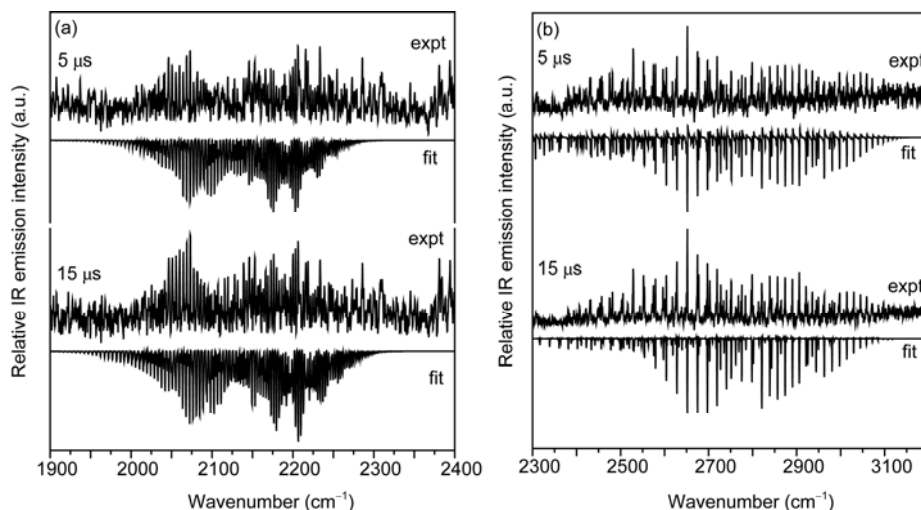| Time (µs)	HCl		CO	
	T_v (K)	E_v (kcal mol^{-1})	T_v (K)	E_v (kcal mol^{-1})
2	30171±11707	20.8±1.8	6998±1528	10.7±0.5
5	14058±6348	18.7±0.3	3636±677	7.4±0.7
15	6828±1350	12.6±0.4	2630±76	5.7±0.2
25	6807±1610	12.6±0.5	2574±243	5.7±0.2
35	6182±1338	11.9±0.5	2524±149	5.6±0.2
45	5856±1187	11.4±0.5	2379±677	5.9±0.3

Figure 2 Representative spectral fitting results for the IR emission bands of the products CO (a) and HCl (b) 45 µs after the photolysis laser shot.
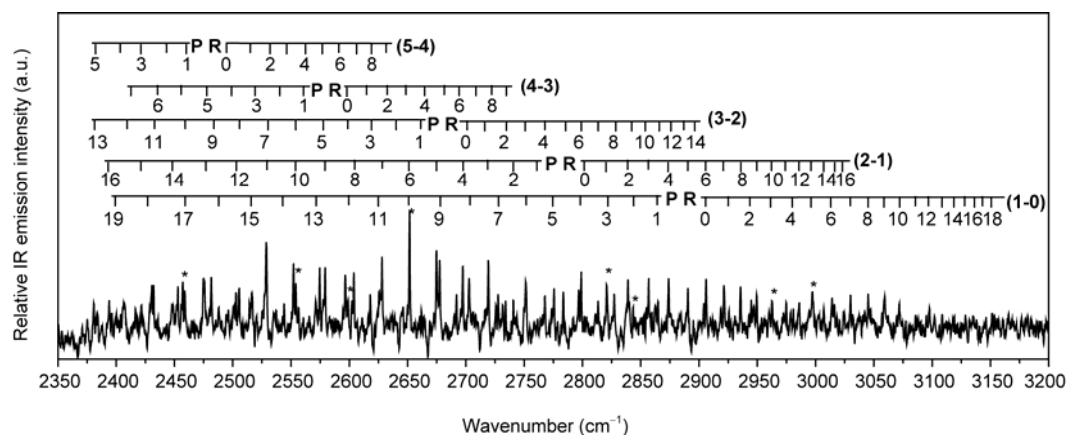

Figure 3 High-resolution emission spectra of HCl in the region 2350–3200 cm^{-1}, averaged 0–5 µs after photolysis of CH$_2$CHCOCl (0.05 torr) in Ar (0.06 torr). Spectral resolution was set at 0.5 cm^{-1}. Assignments are shown as stick diagrams. Partially overlapping lines are indicated by an asterisk.
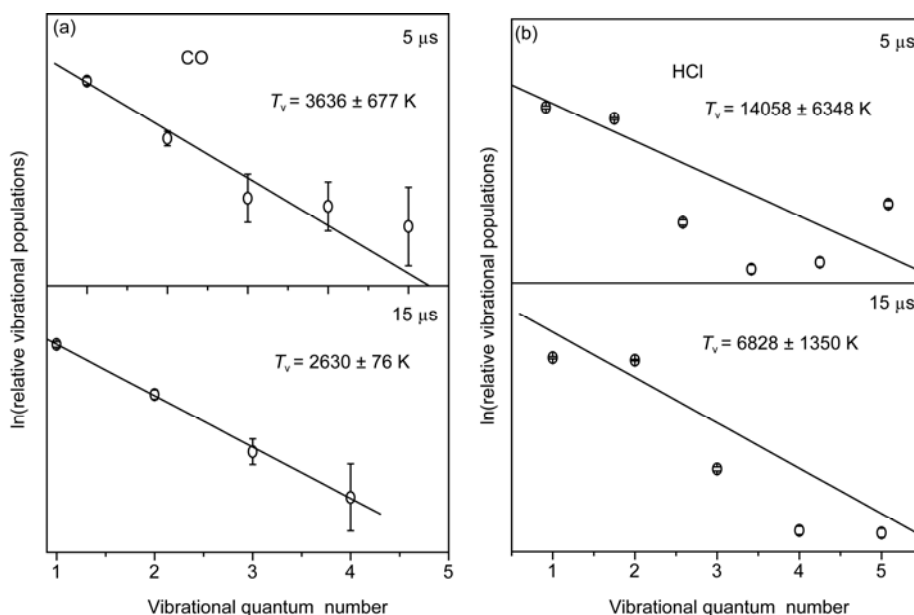
Figure 4　Boltzmann vibrational state distributions of CO (a) and HCl (b) at 5 and 15 μs after photolysis.

very close to the nascent value since nearly collisionless conditions are attained at 2 μs. In view of the vibrational temperature, nascent HCl molecules are partitioned with large vibrational excitation but this is not the case for CO molecules. At later delay times, both HCl and CO undergo vibrational relaxation to some extent due to collisions with the precursor molecules.

3.3　Photodissociation channels and mechanisms

As an α,β unsaturated carbonyl compound containing the enone group –C=C–C=O, $CH_2CHCOCl$ is a bichromophoric molecule which exhibits two absorption bands peaking at about 270 nm and 200 nm, corresponding to the dipole forbidden transition to the $S_1(n\pi^*)$ state and the strongly dipole allowed transition to the $S_2(\pi\pi^*)$ state, respectively [21]. Although 193 nm excitation affords $CH_2CHCOCl$ in its S_2 state, the S_2 state adiabatically correlates only with (energetically unavailable) highly excited photoproducts and therefore, as no fluorescence is observed, is assumed to rapidly internally convert to the lower lying S_1 state, where the photodissociation is initiated.

With TR-FTIR emission spectroscopy, the photodissociation channels and mechanisms can be elucidated by identifying the photofragments (CO, HCl and C_2H_2) and analyzing their internal energies (rotation and vibration).

Clearly, HCl and C_2H_2 are formed in the molecular elimination channel (2) which gives rise to HCl + propadienone (CH_2CCO). The metastable CH_2CCO dissociates further to CO + vinylidene (CH_2C:) and CH_2C: readily rearranges to C_2H_2 through the well-known vinylidene-acetylene isomerization with a barrier [22] of only 1.5 kcal mol^{-1}. This channel was suggested by Butler *et al.* [8] to

occur through a four-center molecular elimination mechanism in the highly vibrationally excited ground electronic state following internal conversion from the S_1 state to the S_0 state, as shown in Figure 5. Their argument was based mainly on the expected large vibrational excitation of HCl when produced from the four-center elimination with the transition-state possessing a long HCl bond length (calculated to be 1.87 Å in this work at the B3LYP/6-311G (d,p) level as shown in Figure 6). However, they only indicated HCl to have considerable vibrational excitation, although
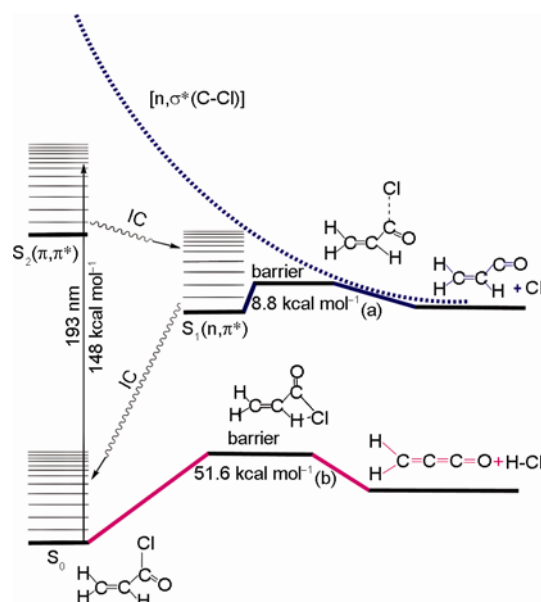

Figure 5　Schematic photophysical and photochemical processes following 193 nm excitation of acryloyl chloride in the gas phase. The reaction barrier of (a) is adapted from ref. [15], while the reaction barrier of (b) is obtained by CCSD(T)//B3LYP/6-311G (d,p) calculations in this work.

the internal energy could be estimated to be roughly 23 kcal mol^{-1} through their measurement of the translational energy. Here in this work, the vibrational and rotational energy of HCl can be determined directly from the TR-FTIR emission spectra, which shows that indeed HCl is highly vibrationally excited (up to $v = 6$) with a vibrational energy of 20.8 kcal mol^{-1}, but much less rotationally excited with the rotational energy being only 3.0 kcal mol^{-1}. Such an energy partition pattern is usually a characteristic of the four-center elimination mechanism [23]. Thus, the HCl four-center elimination mechanism can be firmly established on the basis of the current experimental data. On the other hand, the mechanism in Scheme 1 proposed on the basis of the Ar-matrix experiments [11] can be ruled out. If HCl is produced from 3-chloro-1,2-propenone (ClCH$_2$–CH=C=O) following the 1,3-Cl migration of CH$_2$CHCOCl, as shown in Scheme 1, a three-center elimination mechanism is expected which should produce highly rotationally excited HCl up to $J_{max} = 42$ [20]. This is just the opposite of our experimental observation that HCl possesses only low rotational excitation ($J_{max} = 19$). Thus, it is not likely that HCl arises from the further dissociation of 3-chloro-1,2-propenone (ClCH$_2$–CH=C=O).

It is noteworthy that the sum of the vibrational and rotational energy gives 23.8 kcal mol^{-1} as the total internal energy of HCl, which is consistent with the value of 23 kcal mol^{-1} estimated by Butler *et al.* [8] Accordingly, the internal energy of the co-fragment propadienone should be greater than 37 kcal mol^{-1} since the estimated overall internal energy of HCl and propadienone was greater than 60 kcal mol^{-1} [8]. Qualitatively, this is sufficient to overcome the calculated barrier [8] of 39.5 kcal mol^{-1} leading to further dissociation to give CH$_2$C: (C$_2$H$_2$) + CO. As observed in the TR-FTIR spectra shown in Figure 1, strong IR emission bands due to the photoproducts C$_2$H$_2$ and CO are clearly identified along with HCl.

The third photoproduct CO may arise from several possible channels. Besides the above discussed HCl elimination channel (2) giving rise to propadienone CH$_2$CCO which fragments into CH$_2$C: (C$_2$H$_2$) + CO, there are also another two channels yielding CO, i.e., the C–Cl bond fission channel (1) yielding Cl + propenoyl radical (CH$_2$CHO) with the secondary dissociation of the propenoyl radical giving CH$_2$CH + CO, and the C–C bond fission channel (3) producing CH$_2$CH + ClCO with ClCO dissociating concertedly to Cl + CO. The potential energy surfaces of these two bond fission channels occurring in the excited S$_1$ state have been mapped with the aid of combined CASSCF and MR-CI calculations [15] from which it was revealed that the C–Cl bond fission is more facile than the C–C bond fission because the barrier for the former is only 8.8 kcal mol^{-1} but is 51.7 kcal mol^{-1} for the latter. This can be understood since fission of the C–C bond α to the carbonyl group should proceed with great difficulty since the π conjugation of

CH$_2$CHCOCl enhances the C–C bond strength so that it has some double-bond character. Therefore, cleaving of the C–Cl bond instead of the C–C bond is more favorable upon 193 nm excitation. The C–C bond fission channel (3) is not likely to be a source of the photofragments CO. The C–Cl fission channel (1) and the HCl elimination channel (2) should account for the yield of CO in this experiment. Both channels are characterized by the further dissociation of primary photofragments to produce CO and hence CO is expected to be partitioned with low energy. In fact, our data show that CO is only moderately vibrationally and rotationally excited with a vibrational energy of 10.7 kcal mol^{-1} and rotational energy of 7.9 kcal mol^{-1}. It is not possible to distinguish these two channels, as CO exhibits one set of rovibrational state distribution in the TR-FTIR emission spectra.

Overall, two photochemical reaction channels following the 193 nm excitation of CH$_2$CHCOCl in the gas phase can be identified through the current experiment, i.e., the C–Cl fission channel (1) and the HCl elimination channel (2). There is no evidence for the existence of the 1,3-Cl migration reaction channel (4) in the gas phase. These observations agree well with Butler's experiments [8].

The potential energy surface calculations [15] showed that the 1,3-Cl migration most likely takes place in the triplet T$_1$ state since the barrier of 18.4 kcal mol^{-1} for T$_1$ is much lower than that for the S$_0$ state, 41.8 kcal mol^{-1}. To identify the reactive excited state, our group have also examined specifically the photoinduced 1,3-Cl migration of CH$_2$CHCOCl in solution by TR-FTIR absorption spectroscopy [21]. We found that the major photochemical reaction of CH$_2$CHCOCl at 193 nm in solution is the 1,3-Cl migration accounting for 66% of the product yield, while the C–Cl fission channel only accounts for 32% yield. By monitoring the variation of product yields with the laser excitation wavelength (193 and 266 nm) or the addition of a triplet quencher, the photochemical 1,3-Cl migration reaction was confirmed to take place through the low barrier triplet state T$_1$, rather than the excited singlet state S$_1$ or T$_2$ states with higher barriers.

Considering that the 1,3-Cl migration occurs through the T$_1$ state, the reason why it is absent whereas C–Cl fission and HCl elimination are observed as major photochemical reactions in the gas phase can be understood. The adiabatic and nonadiabatic rate constants as a function of transition energy were calculated[15] which showed that at high transition energy, such as 124.4 kcal mol^{-1}, the C–Cl bond fission in S$_1$ state is the fastest process ($k \approx 1.4 \times 10^{13}$ s^{-1}), as compared to the internal conversion from S$_1$ to S$_0$ ($k \approx 3.6 \times 10^{10}$ s^{-1}) and the intersystem crossing from S$_1$ to T$_1$ ($k \approx 2.9 \times 10^8$ s^{-1}). Thus, the 1,3-Cl migration occurring in the T$_1$ state is rate-limited by the slow S$_1 \rightarrow$ T$_1$ intersystem crossing and cannot compete with the other two reactions, the C–Cl fission in the S$_1$ state and the HCl elimination following the S$_1 \rightarrow$ S$_0$ internal conversion. Of these, the C–Cl

fission in the S_1 state is the major reaction considering its faster rate and this can be confirmed by the relative yield of [Cl]/[HCl] of roughly 3.18 derived from Butler's experiment [8]. Theoretical calculations [15] predicted the C–Cl bond fission to be the exclusive channel upon photolysis at 230 nm and shorter wavelength, based on the calculated rate constants which showed that C–Cl bond fission is 2–3 orders of magnitude faster than that of internal conversion. But both our experiment and Butler's experiment clearly showed that besides the major C–Cl fission channel, there is considerable yield from the HCl elimination channel resulting from the internal conversion processes. In addition to the HCl channel occurring through internal conversion, another minor branch was also suggested to proceed in the ground state after internal conversion producing low kinetic energy Cl atoms [8]. Thus, the $S_1 \rightarrow S_0$ internal conversion also plays an important role in the gas phase photolysis of acryloyl chloride. The main photophysical and photochemical processes following 193 nm excitation of acryloyl chloride can be summarized in Figure 5. In addition to the major photodissociation channel of C–Cl bond fission through the S_1 state or predissociated upper states, the four-center HCl elimination channel following $S_1 \rightarrow S_0$ internal conversion also contributes considerably to the overall gas phase photochemical reactions of $CH_2CHCOCl$.

4   Conclusion

In this work, we have examined the 193 nm photodissociation dynamics of $CH_2CHCOCl$ in the gas phase. With the technique of TR-FTIR emission (TR-FTIR) spectroscopy, vibrationally excited phtotofragments of CO ($v \leqslant 5$), HCl ($v \leqslant 6$), and C_2H_2 are observed. The vibrational and rotational state distribution of the photofragments CO and HCl are acquired by analyzing their fully rotationally resolved $v \rightarrow v-1$ rovibrational progressions in the emission spec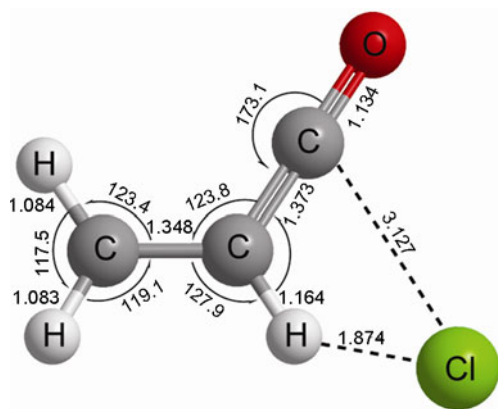tra. CO mainly arises from the secondary dissociation of primary photofragments, either the propenoyl radical (CH_2CHO) from the C–Cl bond fission channel (1) or propadienone (CH_2CCO) from the HCl elimination channel (2), and hence CO is only partitioned with low vibrational energy (10.7 kcal mol^{-1}) and rotational energy (7.9 kcal mol^{-1}). On the other hand, HCl is highly vibrationally excited with the vibrational energy being 20.8 kcal mol^{-1}, but much less rotationally excited with the rotational energy being only 3.0 kcal mol^{-1}. This observation provides direct experimental evidence that HCl is produced from the four-center molecular elimination of $CH_2CHCOCl$ after its internal conversion from the S_1 state to the S_0 state. The gas phase 193 nm excitation of acryloyl chloride mainly leads to two photodissociation channels, the C–Cl fission channel and the HCl elimination channel. In addition to the dominant C–Cl bond fission through the excited S_1 state or upper predissociated states, the $S_1 \rightarrow S_0$ internal conversion is also found to play an important role in the gas phase photolysis of $CH_2CHCOCl$ as manifested by the considerable yield of HCl.

1   Wortelboer HM, Usta M, Zanden JJ, Bladeren PJ, Rietjens IMCM, Cnubben NHP. Inhibition of multidrug resistance proteins MRP1 and MRP2 by a series of α,β-unsaturated carbonyl compounds. *Biochem Pharmacol*, 2005, 69: 1879–1890

2   Billard T. Synthetic applications of β-fluoroalkylated α,β-unsaturated carbonyl compounds. *Chem Eur J*, 2006, 12: 974–979

3   Guerin DJ, Miller SJ. Asymmetric azidation–cycloaddition with open-chain peptide-based catalysts: A sequential enantioselective route to triazoles. *J Am Chem Soc*, 2002, 124: 2134–2136

4   Brocksom TJ, Coelho F, Depres JP, Greene AE, de Lima MEF, Hamelin O, Hartmann B, Kanazawa AM, Wang YY. First comprehensive bakkane approach: Stereoselective and efficient dichloroketene-based total syntheses of (±)- and (−)-9-acetoxyfukinanolide, (±)- and (+)-bakkenolide A, (−)-bakkenolides III, B, C, H, L, V, and X, (±)- and (−)-homogynolide A, (±)-homogynolide B, and (±)-palmosalide C. *J Am Chem Soc*, 2002, 124: 15313–15325

5   Chatani N, Oshita M, Tobisu M, Ishii Y, Murai S. A GaCl$_3$-catalyzed [4+1] cycloaddition of α,β-unsaturated carbonyl compounds and isocyanides leading to unsaturated γ-lactone derivatives. *J Am Chem Soc*, 2003, 125: 7812–7813

6   Oshita M, Yamashita K, Tobisu M, Chatani N. Catalytic [4+1] cycloaddition of α,β-unsaturated carbonyl compounds with isocyanides. *J Am Chem Soc*, 2005, 127: 761–766

7   Arendt MF, Browning PW, Butler LJ. Emission spectroscopy of the predissociative excited state dynamics of acrolein, acrylic acid, and acryloyl chloride at 199 nm. *J Chem Phys*, 1995, 103: 5877–5885

8   Szpunar DE, Miller JL, Butler LJ, Qi F. 193-nm photodissociation of acryloyl chloride to probe the unimolecular dissociation of CH_2CHCO radicals and CH_2CCO. *J Chem Phys*, 2004, 120: 4223–4230

9   Lau KC, Liu Y, Butler LJ. Probing the barrier for $CH_2CHCO \rightarrow CH_2CH+CO$ by the velocity map imaging method. *J Chem Phys*, 2005, 123: 054322

10   Pietri N, Monnier M, Aycard J-P. Photolysis of matrix-isolated acryloyl chloride: 1,3 Chlorine migration and further evolutions. *J Org Chem*, 1998, 63: 2462–2468

11   Feairheller WR, Katon JE. Vibrational spectra and rotational isomerism in acrylyl (propenoyl) chloride and related α,β-unsaturated acyl halides. *J Chem Phys*, 1967, 47: 1248–1255

Figure 6   Geometries of the four-center transition state involved in the HCl elimination of acryloyl chloride obtained from B3LYP/6-311G(d,p) calculations. Bond distances are in Ångstroms and bond angles are in degrees.

12   Keirns JJ, Curl RF. Microwave spectrum of acryloyl fluoride. *J Chem Phys*, 1968, 48: 3773–3778

13   Durig JR, Church JS, Compton DAC. Low frequency vibrational spectra and internal rotation of 2-chlorobuta-1,3-diene, propenoyl fluoride, and propenoyl chloride. *J Chem Phys*, 1979, 71: 1175–1182

14   Hagen K, Hedberg K. Conformational analysis. 8. Propenoyl chloride. An electron-diffraction investigation of the molecular structure, composition, syn-anti energy and entropy differences, and potential hindering internal rotation. *J Am Chem Soc*, 1984, 106: 6150–6155

15   Cui GL, Li QS, Zhang F, Fang WH, Yu JG. Combined CASSCF and MR-CI study on photoinduced dissociation and isomerization of acryloyl chloride. *J Phys Chem A*, 2006, 110: 11839–11846

16   Xiang TC, Liu KH, Zhao SL, Su HM, Kong FA, Wang BS. Multi-channel reaction of $C_2Cl_3 + O_2$ studied by time-resolved Fourier transform infrared emission spectroscopy. *J Phys Chem A*, 2007, 111: 9606–9612

17   Liu KH, Song D, Zhao SL, Wang SF, Yang CF, Su HM. Competitive reaction pathways of $C_2Cl_3 + NO$ via four-membered ring and bicyclic ring intermediates. *Phys Chem Chem Phys*, 2011, 13: 1990–2000

18   Arunan E, Setser DS, Ogilvie JF. Vibration–rotational Einstein coefficients for HF/DF and HCl/DCl. *J Chem Phys*, 1992, 97: 1734–1741

19   Coxon JA, Roychowdhury UK. Rotational analysis of the $B^1\Sigma+ \rightarrow X^1\Sigma+$ system of $H^{35}Cl$. *Can J Phys*, 1985, 63: 1485–1497

20   Lin S-R, Lin S-C., Lee Y-C, Chou I-C, Chen I-C, Lee Y-P. Three-center versus four-center HCl-elimination in photolysis of vinyl chloride at 193 nm: Bimodal rotational distribution of HCl ($v \leqslant 7$) detected with time-resolved Fourier-transform spectroscopy. *J Chem Phys*, 2001, 114: 160–168

21   Wu WQ, Liu KH, Yang CF, Zhao HM, Wang H, Yu YQ, Su HM. Reaction mechanisms of a photo-induced [1,3] sigmatropic rearrangement via a nonadiabatic pathway. *J Phys Chem A*, 2009, 113: 13892–13900

22   Chang N-Y, Shen M-Y,Yu C-H. Extended *ab initio* studies of the vinylidene-acetylene rearrangement. *J Chem Phys*, 1997, 106: 3237–3242

23   Parsons BF, Butler LJ, Ruscic B. Theoretical investigation of the transition states leading to HCl elimination in 2-chloropropene . *Mol Phys*, 2002, 100: 865–874